Electronic Supplementary Material (ESI) for Journal of Materials Chemistry A.
This journal is © The Royal Society of Chemistry 2024

Supporting Information

Constructing vacancy-rich metal phosphates by the spatial effect of ionic oligomers for enhanced OER activity

Yida Zhao, Xinyu He, Xiaoming Ma, Zhengxi Guo, Menghui Qi, Zhaoming Liu and Ruikang Tang**

Department of Chemistry, Zhejiang University, Hangzhou, Zhejiang 310058, China

E-mail: oldliu@zju.edu.cn, rtang@zju.edu.cn

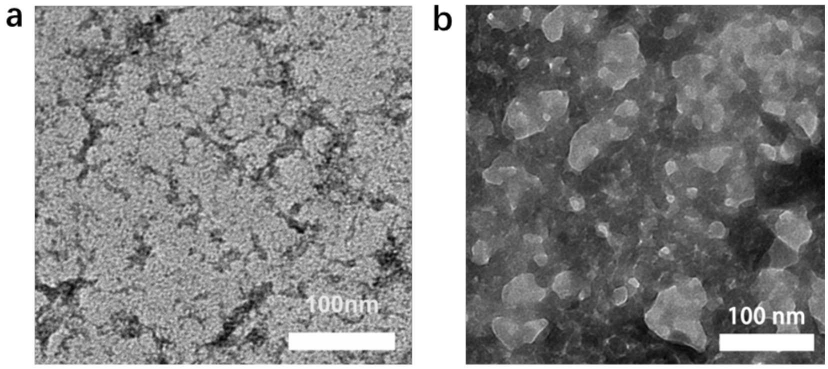

Figure S1. TEM image of A-$Ni_{0.5}Co_{0.5}Pi$ during the synthesis process at different stages. (a) Branch-like structures and (b) porous structures during the process of crosslinking/polymerization.

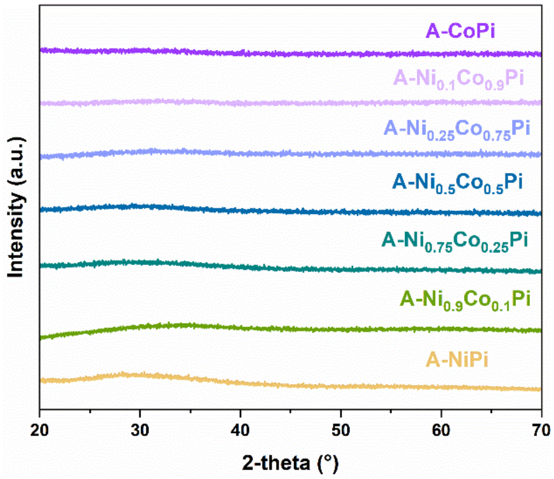

Figure S2. XRD curves of A-NiCoPi with different Ni/Co ratios.

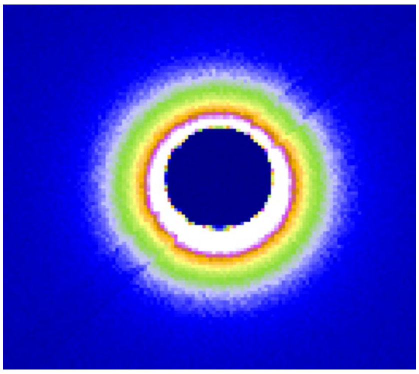

Figure S3. 2D SAXS image of A-$Ni_{0.5}Co_{0.5}Pi$.

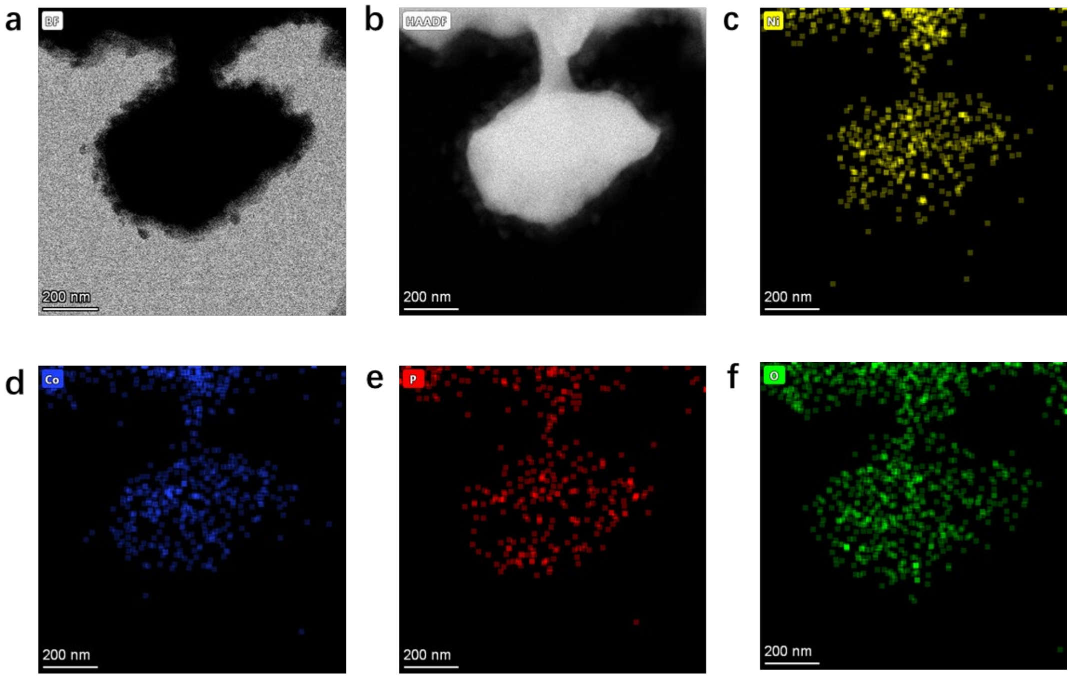

Figure S4. (a) HRTEM image, (b) HAADF-STEM image, (c)-(f) Element mapping of A-$Ni_{0.5}Co_{0.5}Pi$ at large scale.

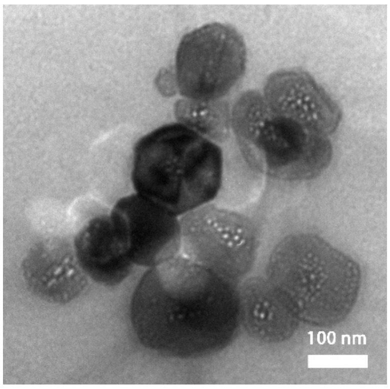

Figure S5. TEM image of C-$Ni_{0.5}Co_{0.5}Pi$.

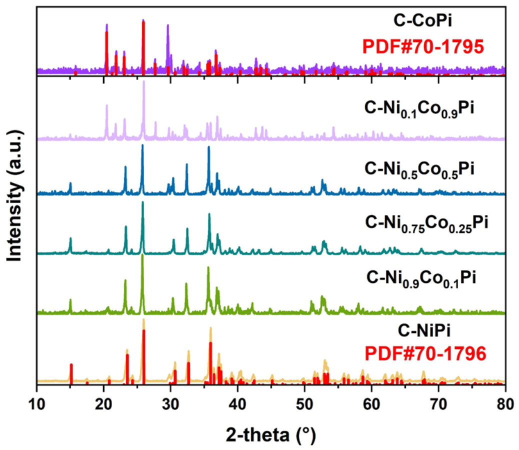

Figure S6. XRD curves of C-NiCoPi with different Ni/Co ratios.

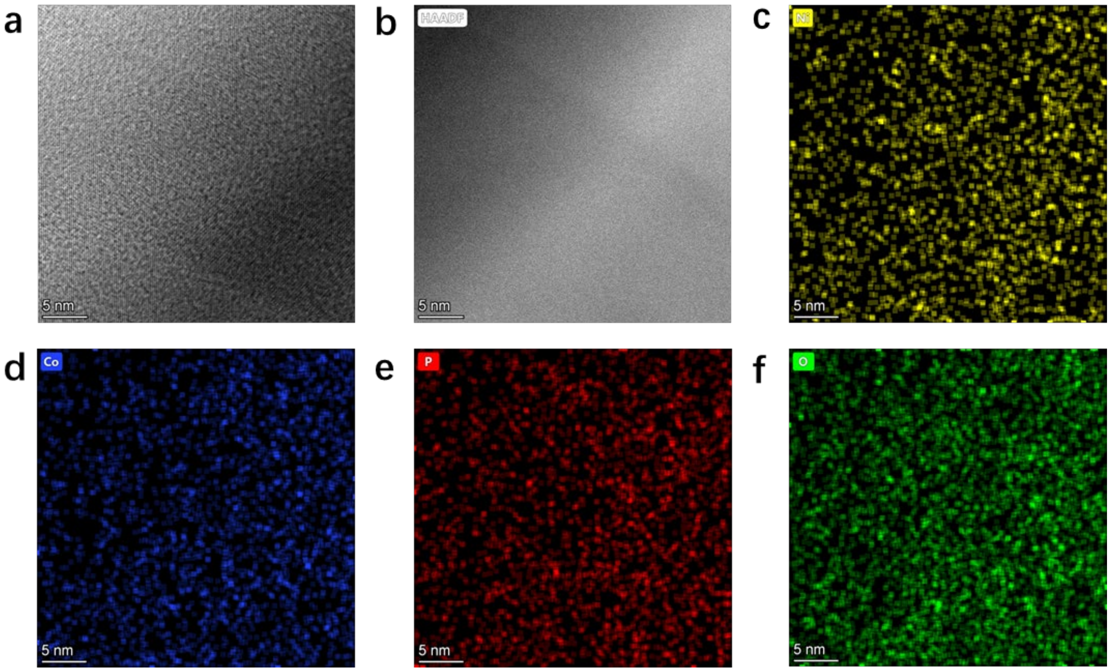

Figure S7. (a) HRTEM image, (b) HAADF-STEM image, (c)-(f) Element mapping of C-$Ni_{0.5}Co_{0.5}Pi$ at nano scale.

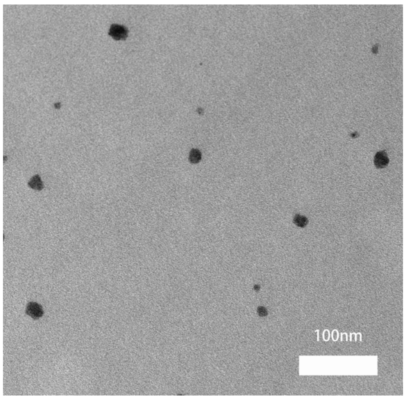

Figure S8. TEM image of N-$Ni_{0.5}Co_{0.5}Pi$.

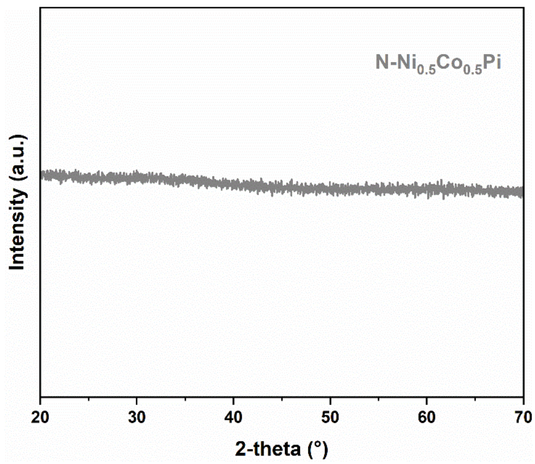

Figure S9. XRD curve of N-$Ni_{0.5}Co_{0.5}Pi$.

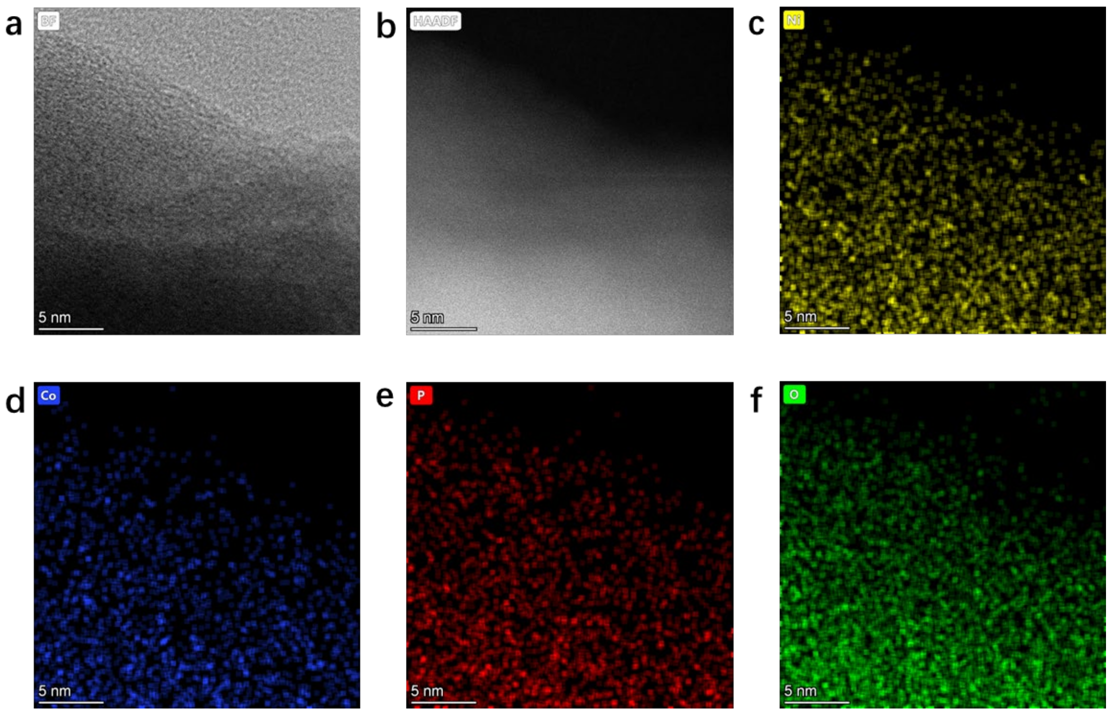

Figure S10. (a) HRTEM image, (b) HAADF-STEM image, (c)-(f) Element mapping of N-$Ni_{0.5}Co_{0.5}Pi$ at nano scale.

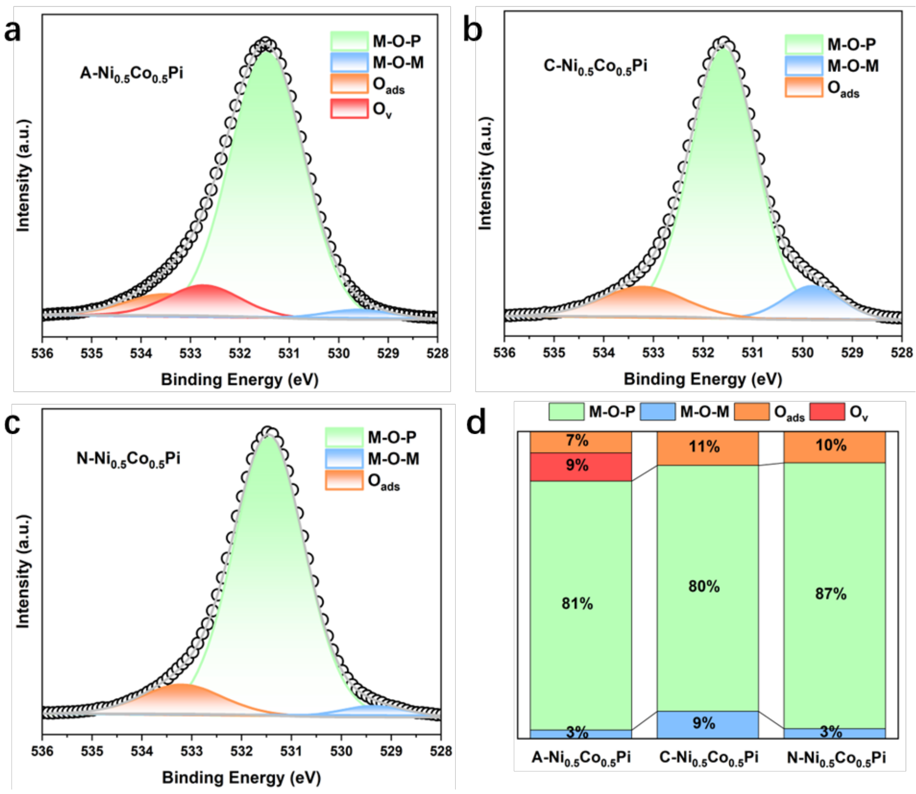

Figure S11. The O1s XPS spectra and the fitting results of (a) A-$Ni_{0.5}Co_{0.5}Pi$, (b) C-$Ni_{0.5}Co_{0.5}Pi$ and (c) N-$Ni_{0.5}Co_{0.5}Pi$. (d) Corresponding contribution analysis.

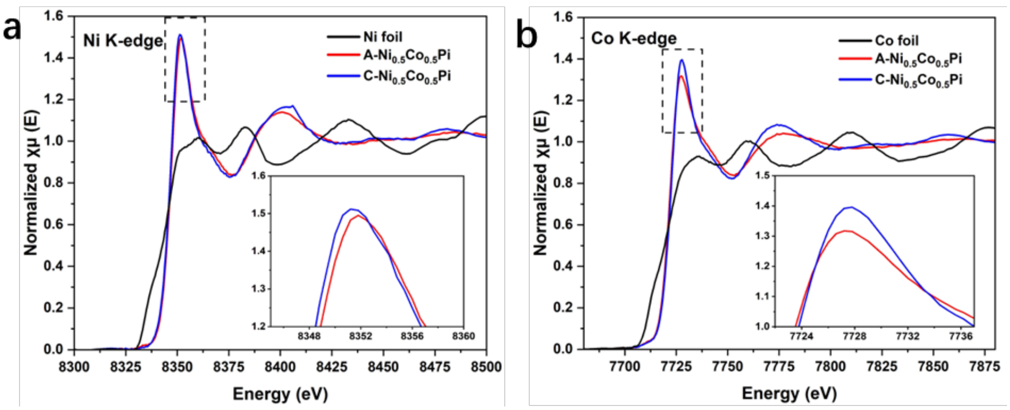

Figure S12. (a) Ni K-edge and (b) Co K-edge XANES spectra comparison of A-$Ni_{0.5}Co_{0.5}Pi$ and C-$Ni_{0.5}Co_{0.5}Pi$.

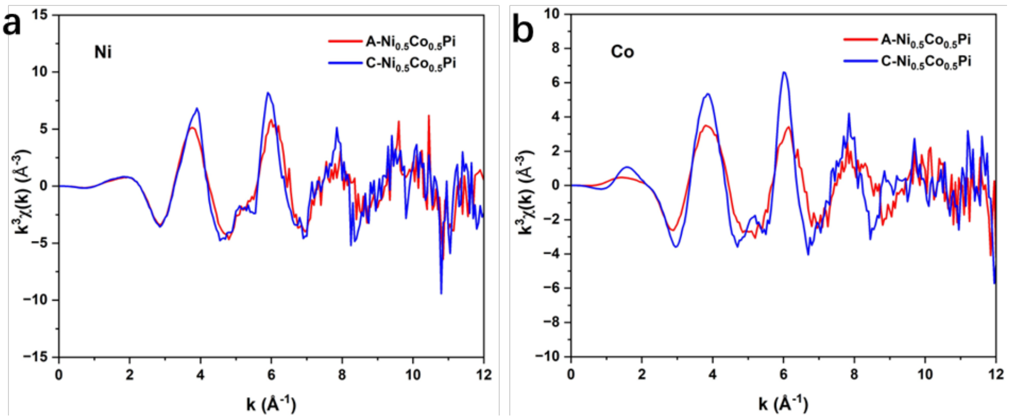

Figure S13. (a) Ni K-edge and (b) Co K-edge EXAFS oscillations comparison of A-$Ni_{0.5}Co_{0.5}Pi$ and C-$Ni_{0.5}Co_{0.5}Pi$ in k space.

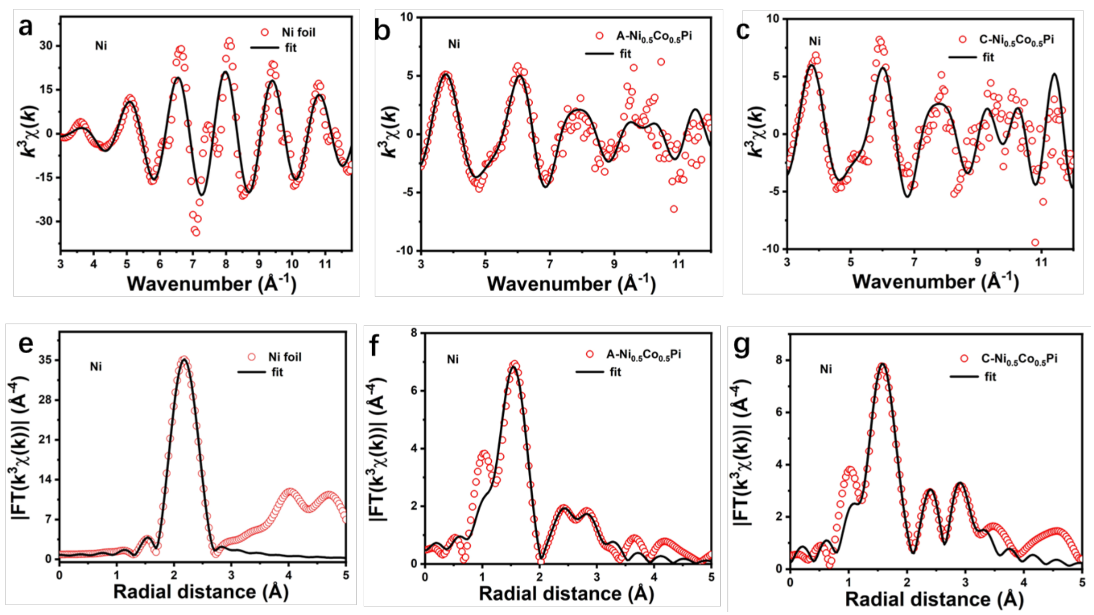

Figure S14. Ni K-edge EXAFS oscillation functions $k^3\chi(k)$ and fitting of (a) Ni foil,

(b) A-$Ni_{0.5}Co_{0.5}Pi$, and (c) C-$Ni_{0.5}Co_{0.5}Pi$. The k^3-weighted FT spectra and fitting in R-space at the Ni K-edge of (d) Ni foil, (e) A-$Ni_{0.5}Co_{0.5}Pi$, and (f) C-$Ni_{0.5}Co_{0.5}Pi$.

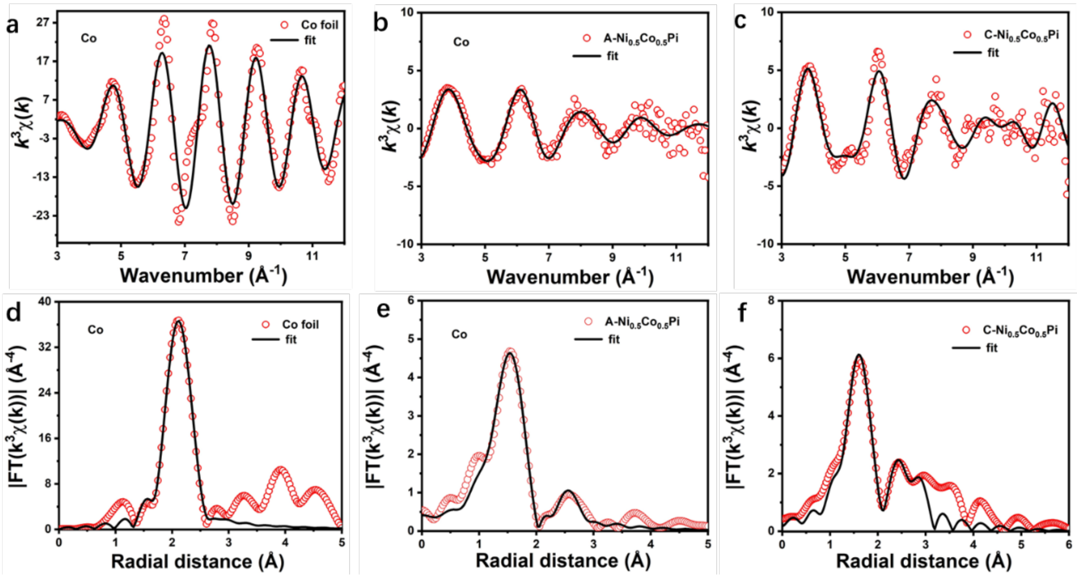

Figure S15. Co K-edge EXAFS oscillation functions $k^3\chi(k)$ and fitting of (a) Co foil, (b) A-$Ni_{0.5}Co_{0.5}Pi$, and (c) C-$Ni_{0.5}Co_{0.5}Pi$. The k^3-weighted FT spectra and fitting in R-space at the Ni K-edge of (d) Co foil, (e) A-$Ni_{0.5}Co_{0.5}Pi$, and (f) C-$Ni_{0.5}Co_{0.5}Pi$.

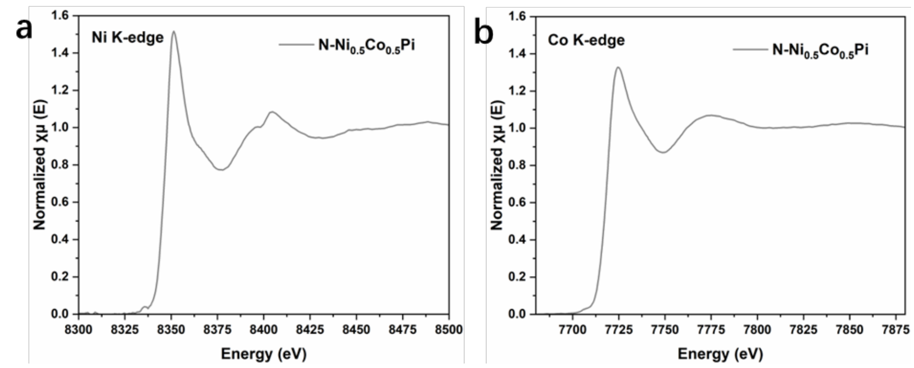

Figure S16. (a) Ni K-edge and (b) Co K-edge XANES spectra of N-$Ni_{0.5}Co_{0.5}Pi$.

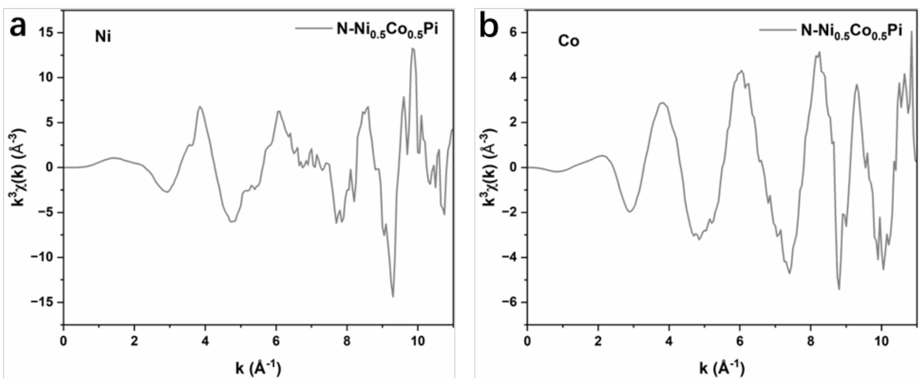

Figure S17. (a) Ni K-edge and (b) Co K-edge EXAFS oscillations of N-$Ni_{0.5}Co_{0.5}Pi$ in k space.

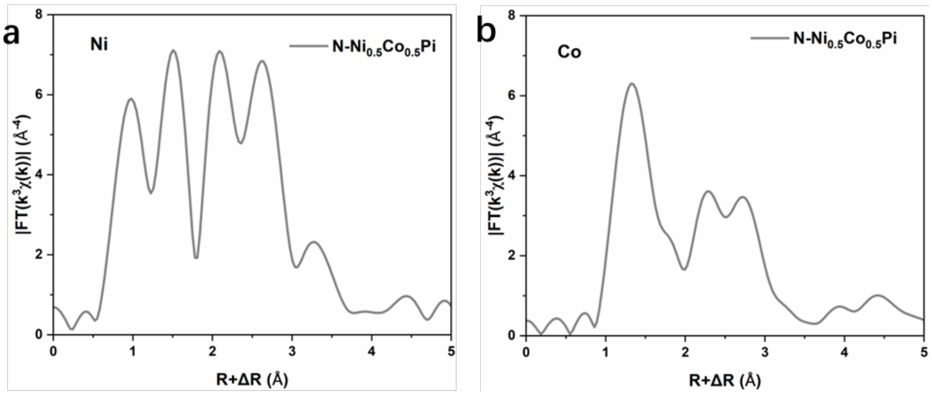

Figure S18. FT curves of the (a) Ni K-edge and (b) Co K-edge EXAFS functions in R-space of N-$Ni_{0.5}Co_{0.5}Pi$.

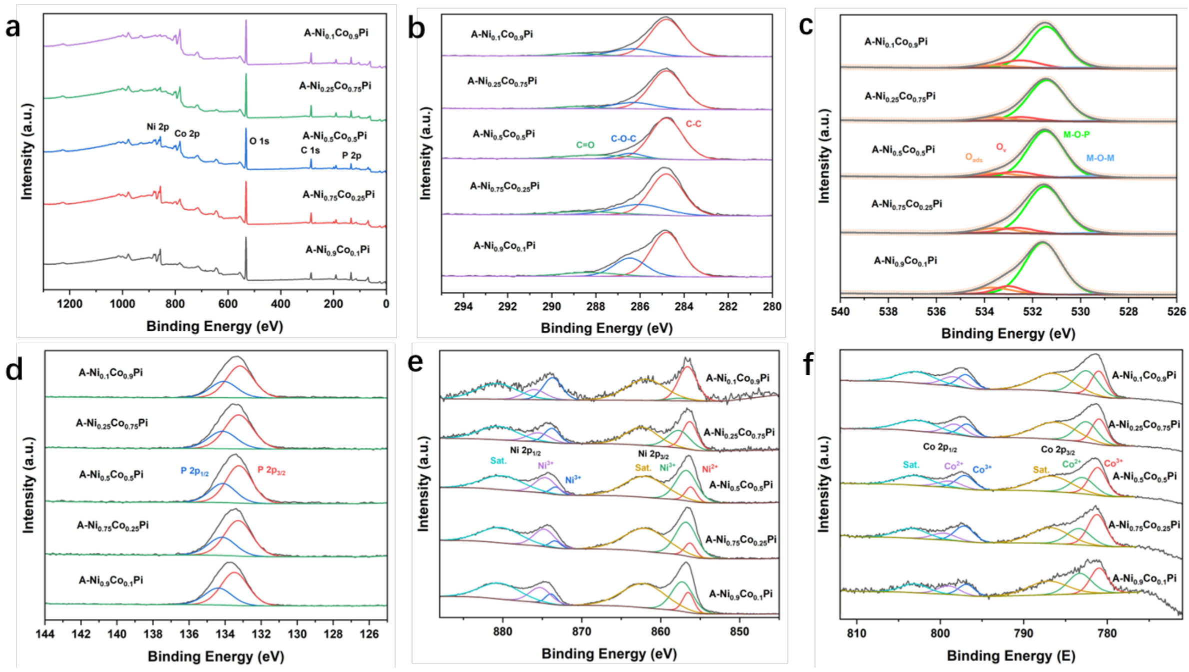

Figure S19. (a) The XPS survey, high-resolution XPS spectra of (b) C 1s, (c) O1s, (d) P 2p, (e) Ni 2p and (f) Co 2p of A-NiCoPi. The spectra distinctly showcase spin-orbit splitting peaks for Ni and Co. Accompanying satellite peaks are also observed. Peaks appearing at 133.5 eV and 134.4 eV are ascribed to the $2p_{3/2}$ and $2p_{1/2}$ levels of P^{5+}, respectively.

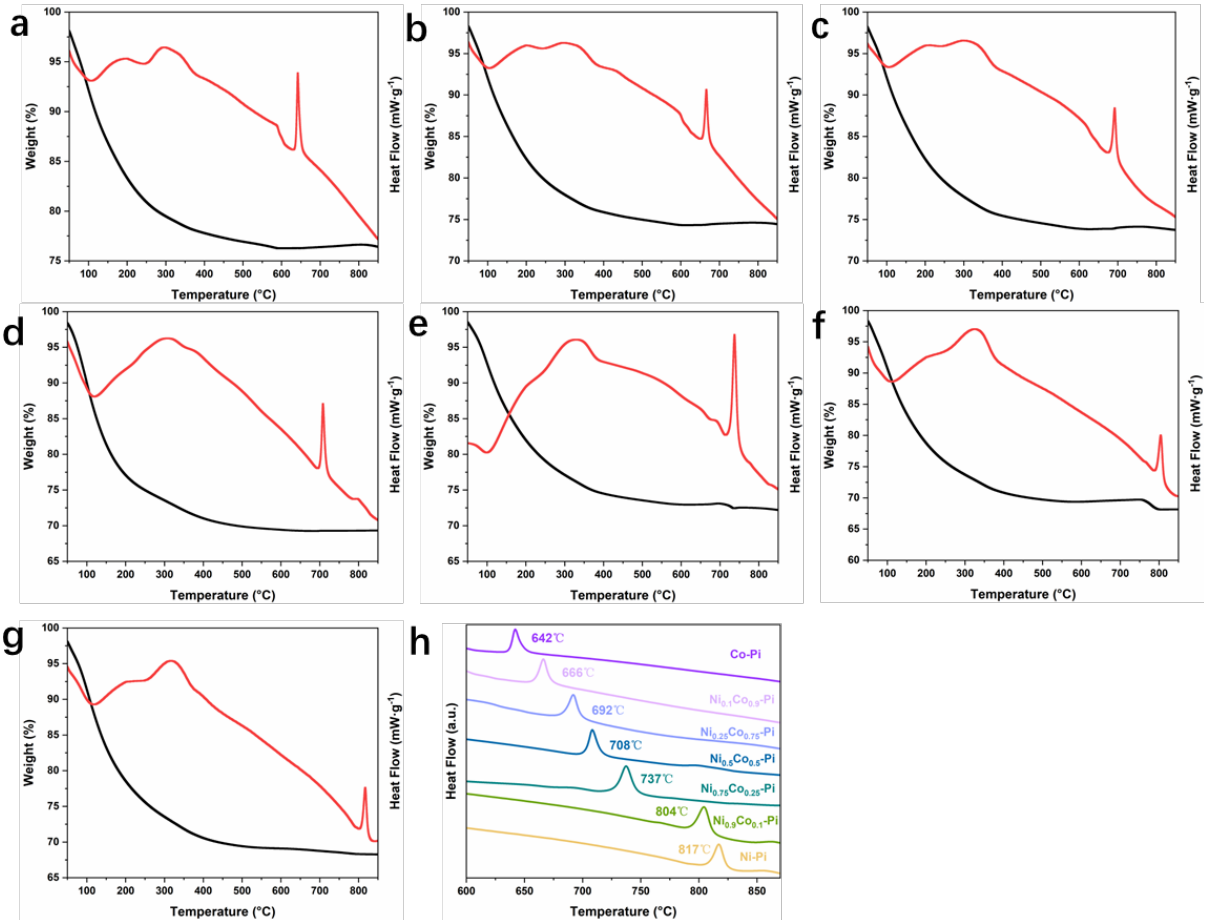

Figure S20. TG/DSC curves of (a) A-CoPi, (b) A-$Ni_{0.1}Co_{0.9}Pi$, (c) A-$Ni_{0.25}Co_{0.75}Pi$, (d) A-$Ni_{0.5}Co_{0.5}Pi$, (e) A-$Ni_{0.75}Co_{0.25}Pi$, (f) A-$Ni_{0.9}Co_{0.1}Pi$ and (g) A-NiPi. (h) DSC curves of A-NiCoPi with different Ni/Co ratios. The crystallization behavior of amorphous materials can reflect their composition and structural information, and multi-stage exothermic crystallization processes are often a characteristic of phase separation. Thermogravimetric/differential scanning calorimetry (TG/DSC) analysis shows that the crystallization peaks of amorphous nickel phosphate (A-NiPi) and amorphous cobalt phosphate (A-CoPi) occur at 817℃ and 642℃, respectively. A-NiCoPi with different Ni/Co ratios exhibit only a single crystallization peak, indicating that their structure is different from simple mixtures and is more homogeneous, resembling the properties of single-phase compounds.

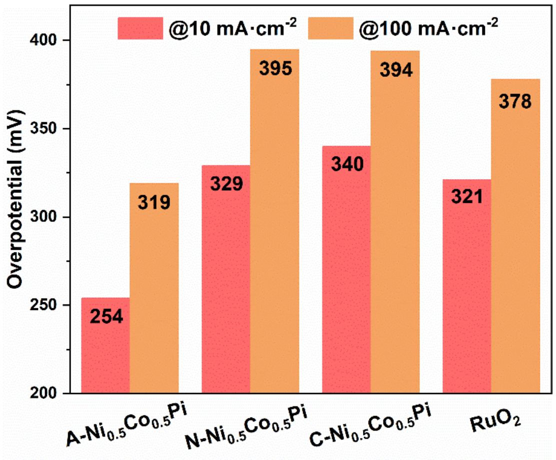

Figure S21. Overpotential comparison of A-$Ni_{0.5}Co_{0.5}Pi$, N-$Ni_{0.5}Co_{0.5}Pi$, C-$Ni_{0.5}Co_{0.5}Pi$ and RuO_2 at 10mA·cm^{-2} and 100mA·cm^{-2}.

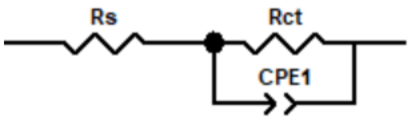

Figure S22. Equivalent circuit model of EIS fitting.

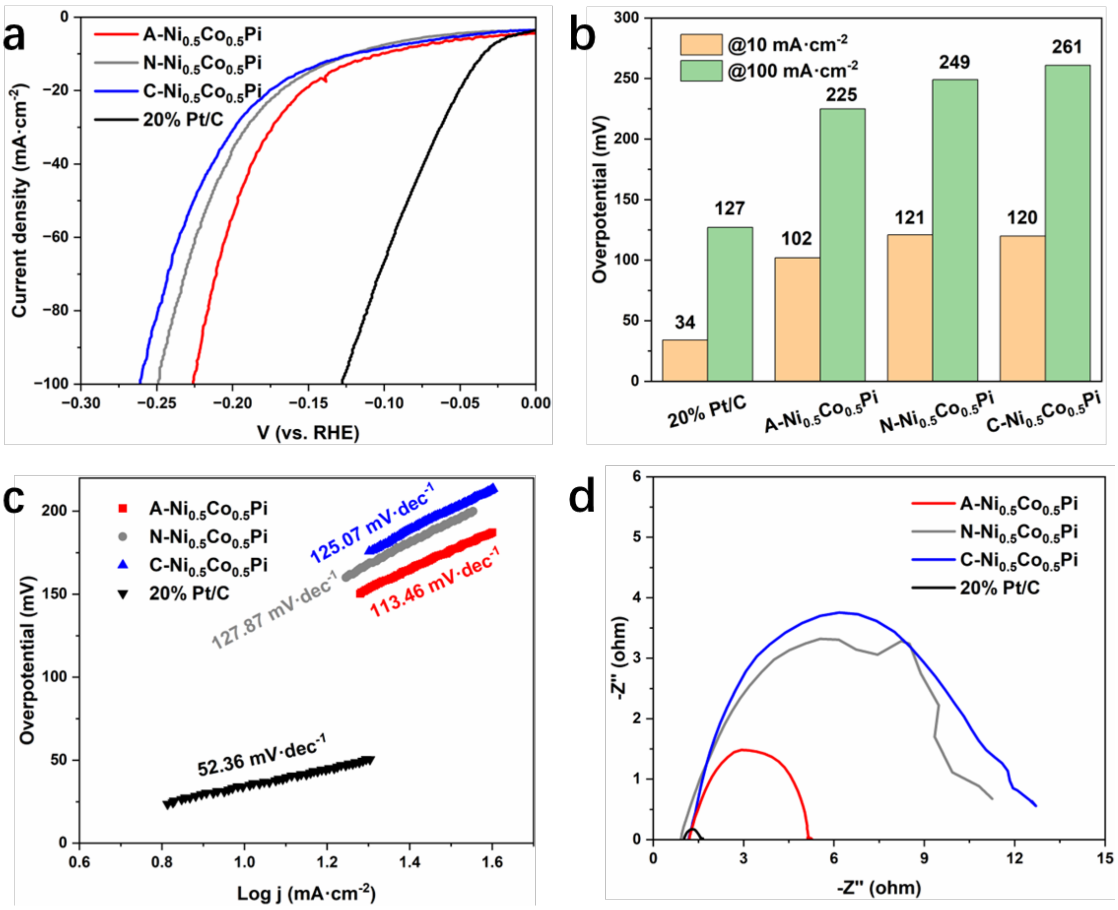

Figure S23. The HER performance of A-$Ni_{0.5}Co_{0.5}Pi$, N-$Ni_{0.5}Co_{0.5}Pi$, C-$Ni_{0.5}Co_{0.5}Pi$ and 20% Pt/C in 1 M KOH. (a) iR-corrected LSV curves of and (b) corresponding Tafel plots. (c) EIS curves at 100 mV overpotential.

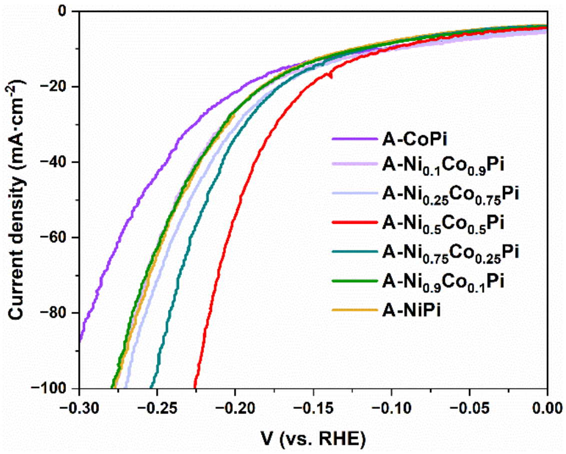

Figure S24. iR-corrected LSV curves of A-NiCoPis' HER performance.

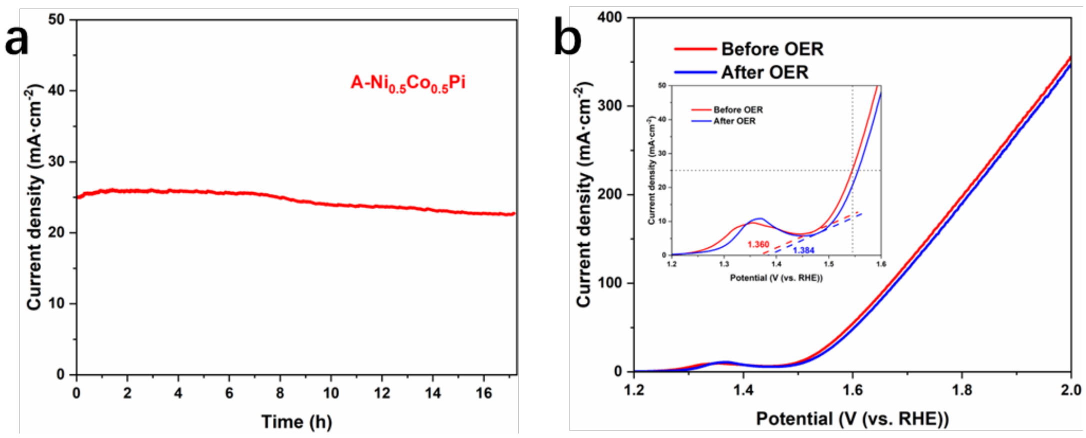

Figure S25. (a) The chronopotentiometry curve of A-$Ni_{0.5}Co_{0.5}Pi$ in 1 M KOH electrolyte at small current density. Average attenuation ratio per hour was 0.6%. (b) Comparison of LSV curves of A-$Ni_{0.5}Co_{0.5}Pi$ before and after stability test.

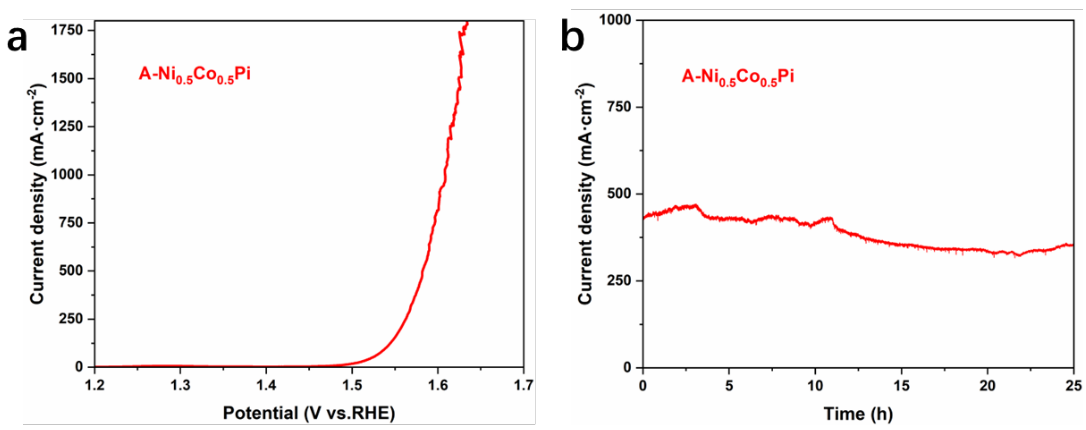

Figure S26. (a) iR-corrected LSV curve and (b) chronopotentiometry curve of

A-Ni0.5Co0.5Pi in 1 M KOH electrolyte under large current density.

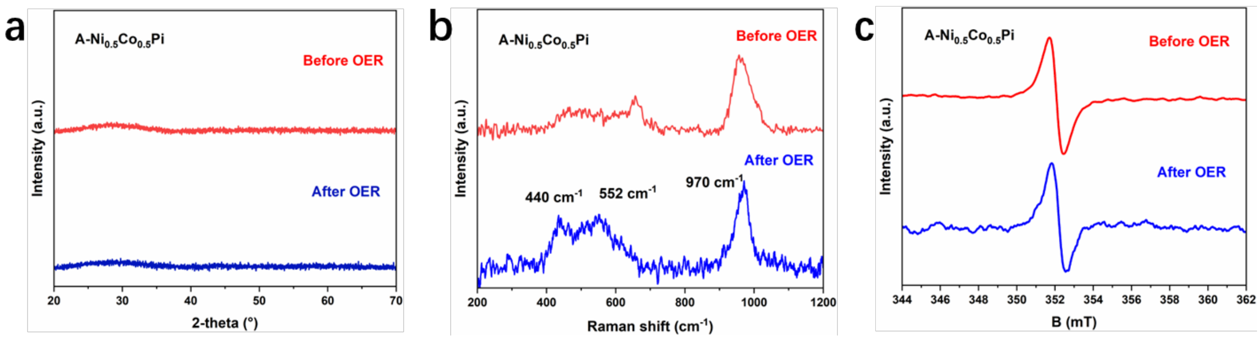

Figure S27. Post stability test of A-$Ni_{0.5}Co_{0.5}$Pi after stability test. (a) XRD, (b) Raman and (c) EPR spectra.

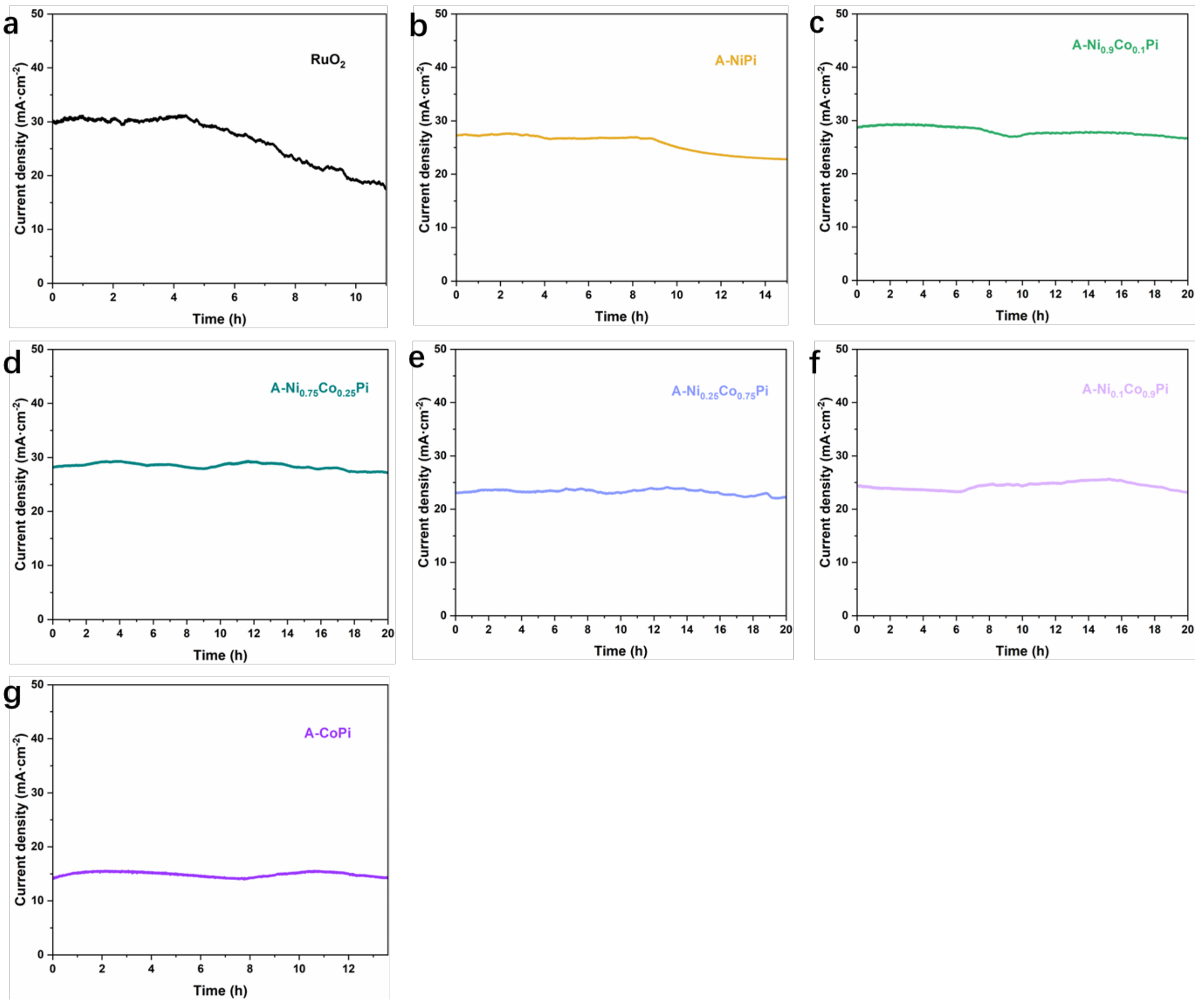

Figure S28. The chronopotentiometry curve of (a) RuO_2, (b) A-NiPi, (c) A-$Ni_{0.9}Co_{0.1}$Pi, (d) A-$Ni_{0.75}Co_{0.25}$Pi, (e) A-$Ni_{0.25}Co_{0.75}$Pi, (f) A-$Ni_{0.1}Co_{0.9}$Pi and (g) A-CoPi in 1 M KOH electrolyte. The slight fluctuations in the i-t curves are attributed to temperature changes.

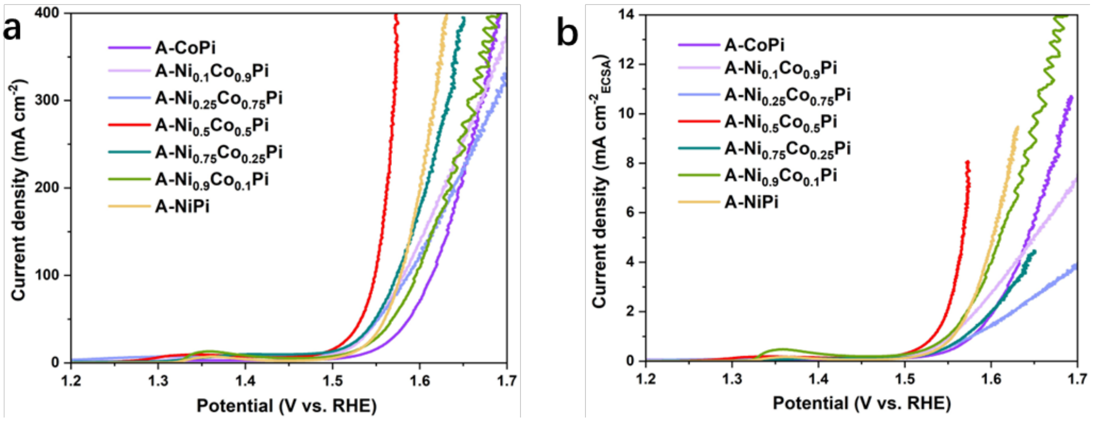

Figure S29. (a) iR-corrected LSV curves and (b) LSV curves normalized by ECSA of A-NiCoPi.

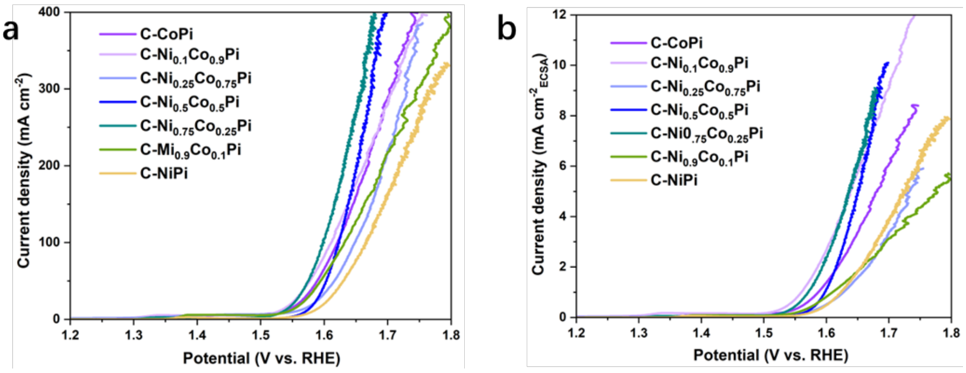

Figure S30. (a) iR-corrected LSV curves and (b) LSV curves normalized by ECSA of C-NiCoPi.

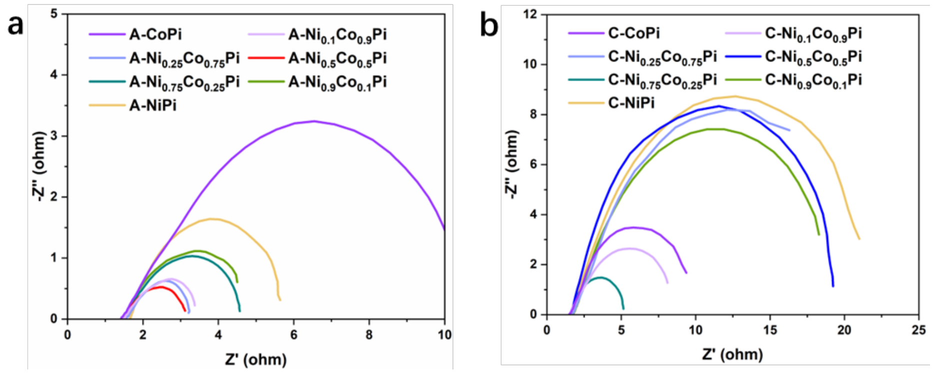

Figure S31. EIS curves of (a) A-NiCoPi and (b) C-NiCoPi.

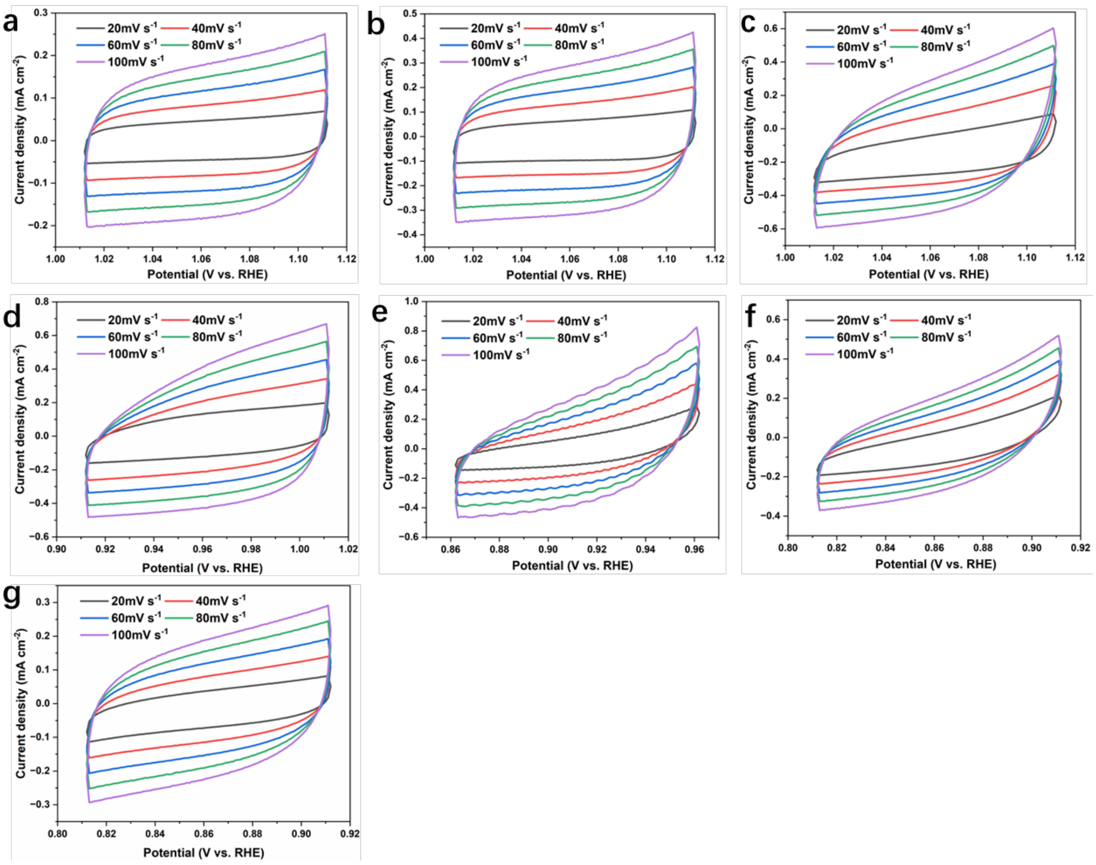

Figure S32. CV curves with different scan rates of (a) A-NiPi, (b) A-$Ni_{0.9}Co_{0.1}Pi$, (c) A-$Ni_{0.75}Co_{0.25}Pi$, (d) A-$Ni_{0.5}Co_{0.5}Pi$, (e) A-$Ni_{0.25}Co_{0.75}Pi$, (f) A-$Ni_{0.1}Co_{0.9}Pi$, (g) A-CoPi.

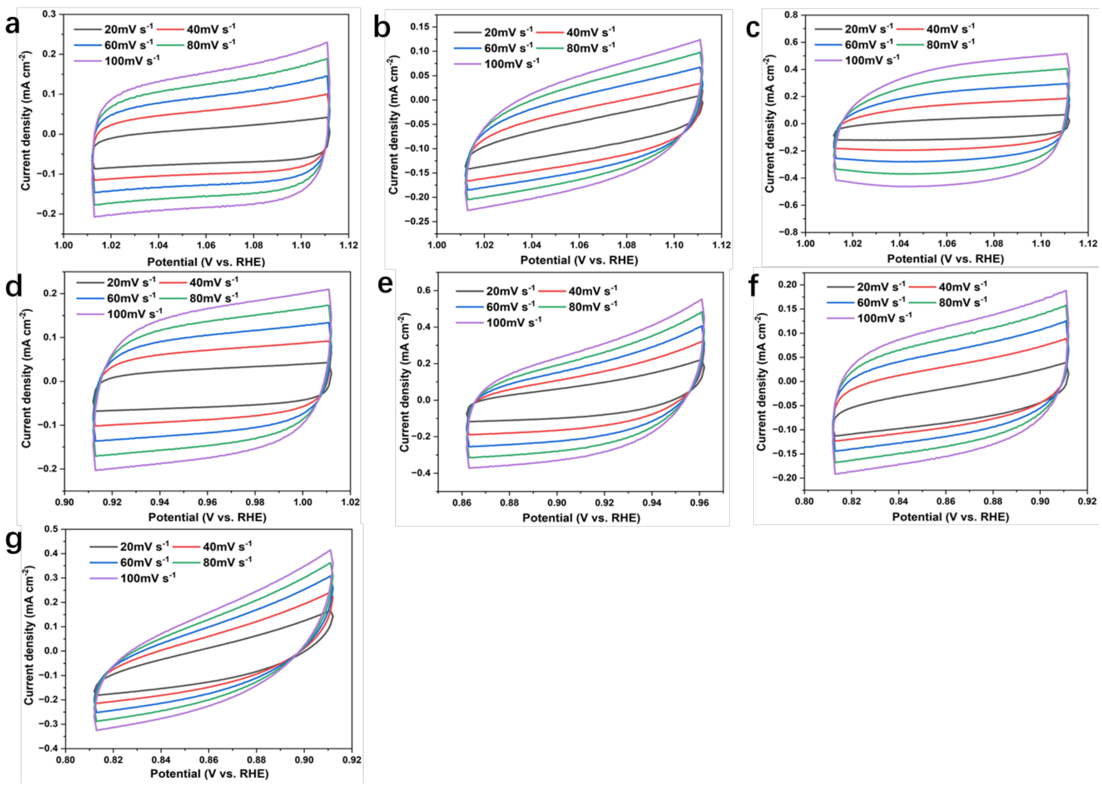

Figure S33. CV curves with different scan rates of (a) C-NiPi, (b) C-$Ni_{0.9}Co_{0.1}Pi$, (c) C-$Ni_{0.75}Co_{0.25}Pi$, (d) C-$Ni_{0.5}Co_{0.5}Pi$, (e) C-$Ni_{0.25}Co_{0.75}Pi$, (f) C-$Ni_{0.1}Co_{0.9}Pi$, (g) C-CoPi.

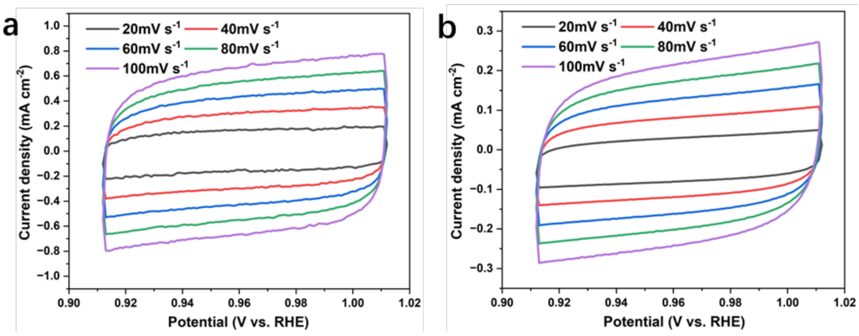

Figure S34. CV curves with different scan rates of (a) RuO_2 and (b) N-$Ni_{0.5}Co_{0.5}Pi$.

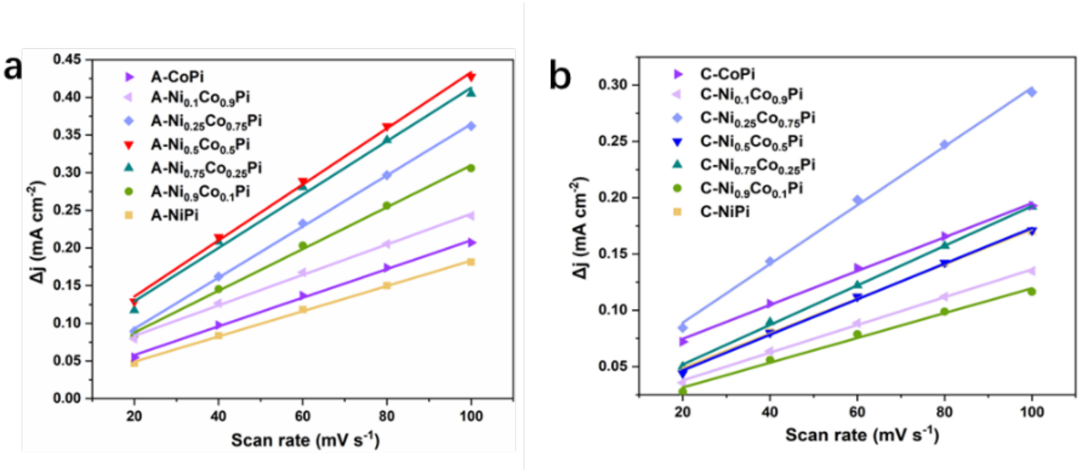

Figure S35. The capacitive current-scan rate plots of (a) A-NiCoPi and (b) C-NiCoPi.

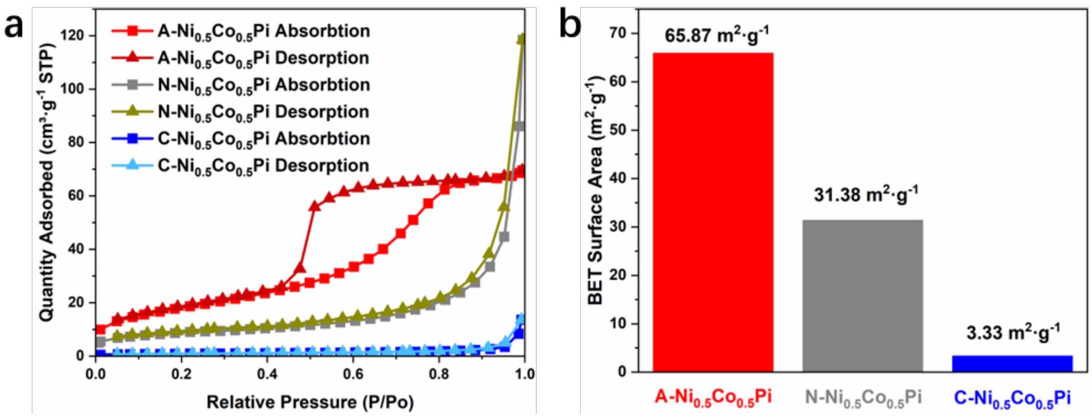

Figure S36. (a) N_2 adsorption/desorption isotherms and (b) the fitted BET Surface Area of A-$Ni_{0.5}Co_{0.5}Pi$, N-$Ni_{0.5}Co_{0.5}Pi$, and C-$Ni_{0.5}Co_{0.5}Pi$.

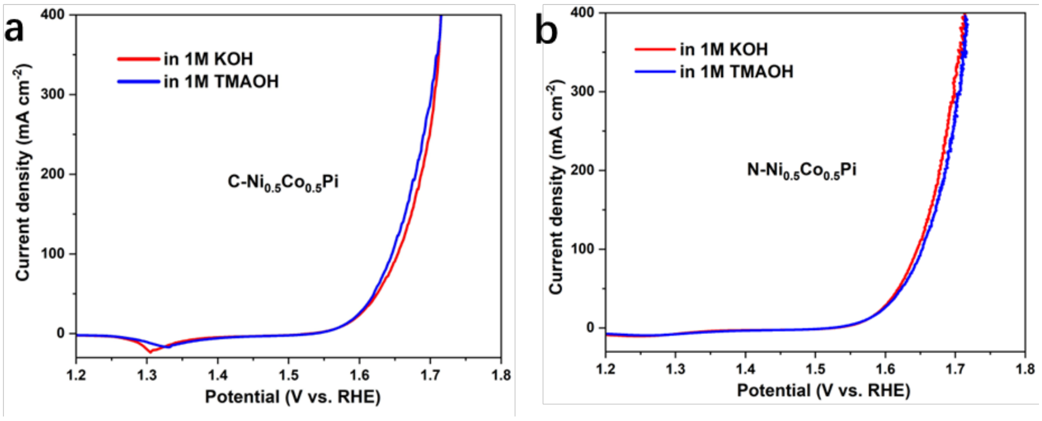

Figure S37. LSV curves of (a) C-$Ni_{0.5}Co_{0.5}Pi$ and (b) N-$Ni_{0.5}Co_{0.5}Pi$ in 1 m KOH and 1 m TMAOH electrolyte.

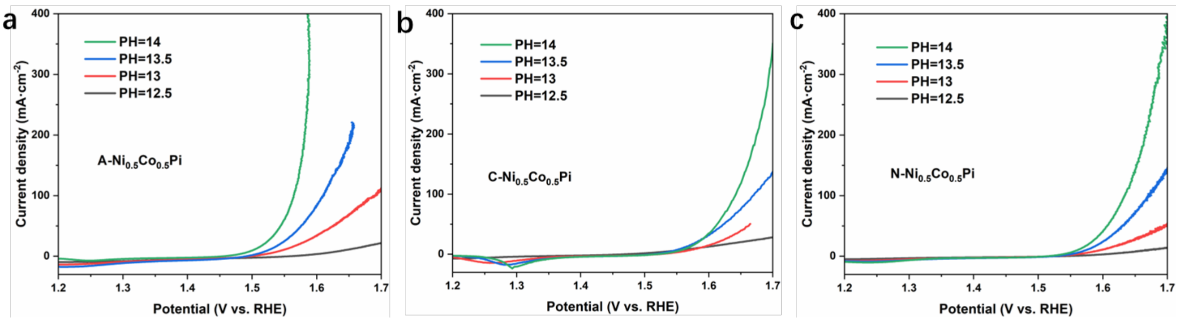

Figure S38. Polarization curves of (a) A-$Ni_{0.5}Co_{0.5}Pi$, (b) C-$Ni_{0.5}Co_{0.5}Pi$ and (c) N-$Ni_{0.5}Co_{0.5}Pi$ in KOH electrolyte with different pH value.

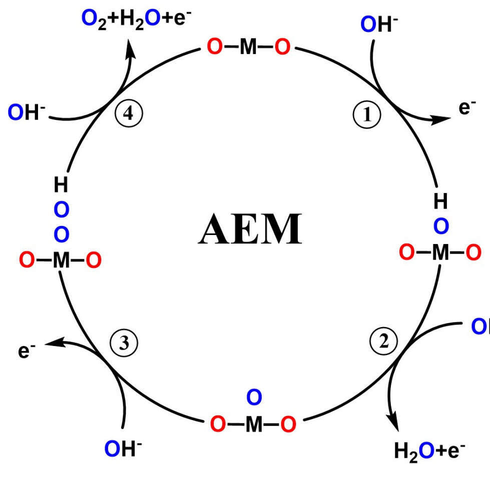

Figure S39. Traditional AEM pathway involving concerted proton–electron transfers on surface metal sites.

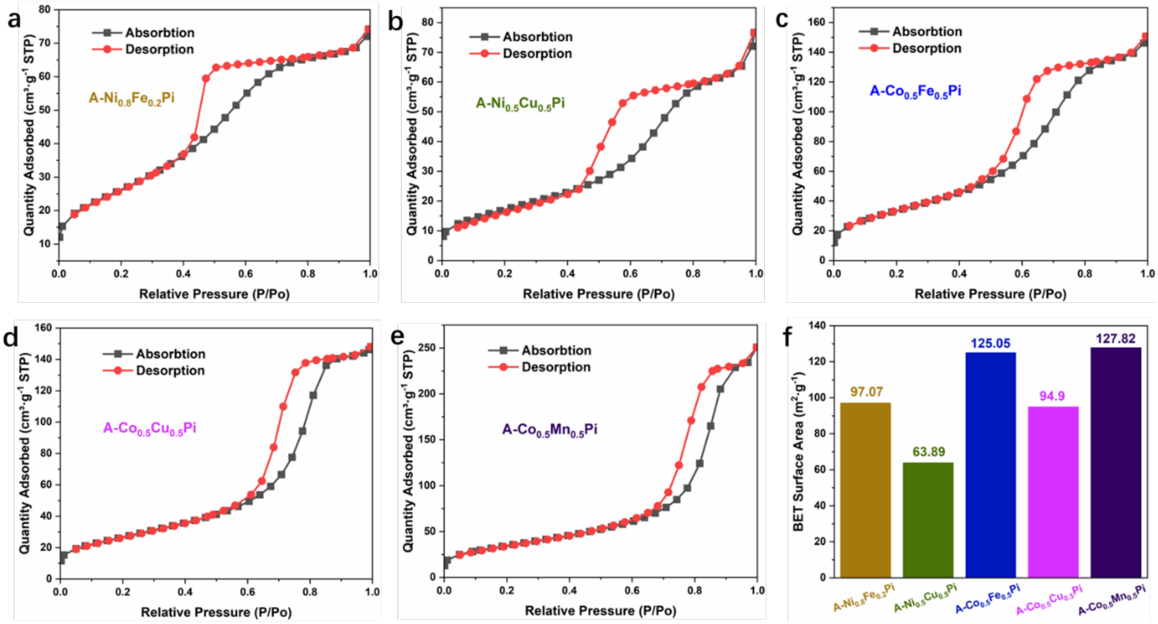

Figure S40. N_2 adsorption/desorption isotherms and (b) the fitted BET Surface Area of A-$Ni_{0.8}Fe_{0.2}$Pi, A-$Ni_{0.5}Cu_{0.5}$Pi, A-$Co_{0.5}Fe_{0.5}$Pi, A-$Co_{0.5}Cu_{0.5}$Pi, and C-$Co_{0.5}Mn_{0.5}$Pi.

Table S1. ICP-AES results of A-NiCoPi with different Ni/Co ratio.

Sample	Feed Ni/Co ratio	Ni content (mg·L^{-1})	Co content (mg·L^{-1})	Real Ni/Co ratio
A-$Ni_{0.9}Co_{0.1}$Pi	9:1	339.7	40.2	8.48:1
A-$Ni_{0.75}Co_{0.25}$Pi	3:1	545.6	188.1	2.91:1
A-$Ni_{0.5}Co_{0.5}$Pi	1:1	317.3	327.9	0.97:1
A-$Ni_{0.25}Co_{0.75}$Pi	1:3	312.2	951.7	1:3.04
A-$Ni_{0.1}Co_{0.9}$Pi	1:9	28.6	263.1	1:8.38
N-$Ni_{0.5}Co_{0.5}$Pi	92:8	31.8	30.4	1.05:1

Table S2. EXAFS fitting parameters at the Co *K*-edge and Ni *K*-edge for various samples. (S_0^2=1.0)

Sample	Path	N^a	R(Å)^b	σ^2(Å^2)^c	ΔE_0(eV)^d	*R* factor
			Co *k*-edge			
Co foil	Co-Co	12.00	2.49 (+/-0.01)	0.0062 (+/-0.0010)	-6.58 (+/-3.05)	0.0097
A-$Ni_{0.5}Co_{0.5}$Pi	Co-O	5.59	2.04 (+/-0.02)	0.0052 (+/-0.0018)	-2.04 (+/0.29)	0.0044
	Co -P	1.13	2.86 (+/-0.03)	0.0072 (+/-0.0009)	9.71 (+/-1.06)	
	Co -Ni/Co	2.11	3.33 (+/-0.02)	0.0031 (+/-0.0015)	3.28 (+/-0.33)	
C-$Ni_{0.5}Co_{0.5}$Pi	Co-O	5.96	2.09 (+/-0.02)	0.0107 (+/-0.0009)	2.68 (+/-1.61)	0.0032
	Co -P	1.23	2.79 (+/-0.03)	0.0048 (+/-0.0002)	9.57 (+/-3.92)	
	Co -Ni/Co	2.58	3.20 (+/-0.03)	0.0035 (+/-0.0003)	9.59 (+/-1.72)	

			Ni *k*-edge			
Ni foil	Ni-Ni	12.00	2.49（+/-0.01）	0.0062（+/-0.0038）	6.06（+/-0.52）	0.0194
	Ni-O	5.61	2.04（+/-0.02）	0.0083（+/-0.0016）	-5.10（+/-3.99）	
A-$Ni_{0.5}Co_{0.5}Pi$	Ni-P	0.88	2.81（+/-0.02）	0.0036（+/-0.0008）	3.23（+/-2.71）	0.0177
	Ni-Ni/Co	0.91	3.17（+/-0.04）	0.0045（+/-0.0006）	9.11（+/-3.77）	
	Ni-O	6.17	2.07（+/-0.02）	0.0080（+/-0.0013）	-6.61（+/-2.93）	
C-$Ni_{0.5}Co_{0.5}Pi$	Ni-P	1.15	2.82（+/-0.02）	0.0082（+/-0.0008）	4.43（+/-1.98）	0.0095
	Ni-Ni/Co	1.00	3.18（+/-0.03）	0.0070（+/-0.0005）	6.74（+/-3.27）	

[a]CN, coordination number; [b]*R*, distance between absorber and backscatter atoms; [c]σ^2, Debye-Waller factor to account for both thermal and structural disorders; [d]ΔE_0, inner potential correction; *R* factor indicates the goodness of the fit. According to the experimental EXAFS fit of Co foil and Ni foil by fixing CN as the known crystallographic value. Fitting range: $3.0 \leq k$ (/Å) ≤ 12.5 and $1.0 \leq R$ (Å) ≤ 3.0 (Co foil); $3.0 \leq k$ (/Å) ≤ 11.8 and $1.0 \leq R$ (Å) ≤ 3.0 (Ni foil); $3.0 \leq k$ (/Å) ≤ 10.7 and $1.0 \leq R$ (Å) ≤ 3.0 (Sample-A-Co) ; $3.0 \leq k$ (/Å) ≤ 11.0 and $1.0 \leq R$ (Å) ≤ 3.0 (Sample-A-Ni) ; $3.0 \leq k$ (/Å) ≤ 11.0 and $1.0 \leq R$ (Å) ≤ 3.0 (Sample-C-Co) ; $3.0 \leq k$ (/Å) ≤ 11.0 and $1.0 \leq R$ (Å) ≤ 3.0 (Sample-C-Ni).

Table S3. Summary of catalytic performance of previously reported OER catalysts in alkaline electrolytes.

Catalyst	η@10 $mA \cdot cm^{-2}$ (mV)	Tafel slope ($mV \cdot dec^{-1}$)	Reference
NPO	380	48	Ref S1[1]
CoPO	350	60.7	Ref S2[2]
CoPi	281	98	Ref S3[3]
Co_2Fe_2-NiPi	300	55	Ref S4[4]
NiCoPi	320	44.5	Ref S5[5]
NiCoPi	310	68	Ref S6[6]
$NiCoHPO_4$	320	84	Ref S7[7]
CNPO	378	60.79	Ref S8[8]
NiCoPi/Ni	273	59.3	Ref S9[9]
NiCoPi	347	35	Ref S10[10]
NFP	330	50	Ref S11[11]
NiFePi/N-C	280	48	Ref S12[12]
NiFePi	240	45	Ref S13[13]
FeCoP/C	282	53	Ref S14[14]
Co-FPOH	290	69	Ref S15[15]
Co:FePi	266	42.6	Ref S16[16]

Co-Fe-P-O	267	30	Ref S17[17]
CoNi-CuHP/NF	299	88	Ref S18[18]
$Co_{0.95}Mn_{0.05}$-Pi	335	84.08	Ref S19[19]
A-$Ni_{0.5}Co_{0.5}$Pi	254	45.75	This work
A-$Ni_{0.8}Fe_{0.2}$Pi	230	51.40	This work
A-$Co_{0.5}Fe_{0.5}$Pi	261	43.23	This work
A-$Ni_{0.5}Cu_{0.5}$Pi	310	55.97	This work
A-$Co_{0.5}Cu_{0.5}$Pi	303	62.18	This work
A-$Co_{0.5}Mn_{0.5}$Pi	307	53.47	This work

References

1. Y. Zhan, M. H. Lu, S. L. Yang, C. H. Xu, Z. L. Liu and J. Y. Lee, *Chemcatchem*, 2016, **8**, 372-379.
2. P. Bhanja, Y. Kim, B. Paul, J. J. Lin, S. M. Alshehri, T. Ahamad, Y. V. Kaneti, A. Bhaumik and Y. Yamauchi, *Chemcatchem*, 2020, **12**, 2091-2096.
3. J. D. Qi, J. F. Xie, Z. M. Wei, S. S. Lou, P. Hao, F. C. Lei and B. Tang, *Chem. Commun.*, 2020, **56**, 4575-4578.
4. H. L. Liu, H. Y. Li and X. Wang, *Small*, 2016, **12**, 2969-2974.
5. L. Yang, H. Ren, Q. H. Liang, K. N. Dinh, R. Dangol and Q. Y. Yan, *Small*, 2020, **16**, 7.
6. N. L. W. Septiani, Y. V. Kaneti, K. B. Fathoni, K. Kani, A. E. Allah, B. Yuliarto, Nugraha, H. K. Dipojono, Z. A. Alothman, D. Golberg and Y. Yamauchi, *Chem. Mater.*, 2020, **32**, 7005-7018.
7. N. L. W. Septiani, Y. V. Kaneti, K. B. Fathoni, Y. N. Guo, Y. Ide, B. Yuliarto, X. C. Jiang, Nugraha, H. K. Dipojono, D. Golberg and Y. Yamauchi, *J. Mater. Chem. A*, 2020, **8**, 3035-3047.
8. D. Wang, Y. J. Wang, Z. Y. Fu, Y. B. Xu, L. X. Yang, F. Wang, X. L. Guo, W. J. Sun and Z. L. Yang, *ACS Appl. Mater. Interfaces*, 2021, **13**, 34507-34517.
9. J. W. Li, W. M. Xu, D. Zhou, J. X. Luo, D. W. Zhang, P. M. Xu, L. C. Wei and D. S. Yuan, *J. Mater. Sci.*, 2018, **53**, 2077-2086.
10. J. C. Zhang, Y. Yang, Z. C. Zhang, X. B. Xu and X. Wang, *J. Mater. Chem. A*, 2014, **2**, 20182-20188.
11. Y. Zhan, M. H. Lu, S. L. Yang, Z. L. Liu and J. Y. Lee, *ChemElectroChem*, 2016, **3**, 615-621.
12. X. Cheng, J. F. Zheng, J. T. Li and X. T. Luo, *ChemElectroChem*, 2019, **6**, 2195-2200.
13. T. Guo, L. J. Zhang, S. Yun, J. D. Zhang, L. T. Kang, Y. X. Li, H. J. Li and A. B. Huang, *Mater. Res. Bull.*, 2019, **114**, 80-84.
14. R. Zhao, B. X. Ni, L. M. Wu, P. C. Sun and T. H. Chen, *Colloids Surf., A*, 2022, **635**, 9.
15. L. T. Song, T. L. Zheng, L. R. Zheng, B. Lu, H. Q. Chen, Q. G. He, W. Z. Zheng,

Y. Hou, J. L. Lian, Y. Wu, J. Chen, Z. Z. Ye and J. G. Lu, *Appl. Catal., B*, 2022, **300**, 10.
16. S. A. Khalate, S. A. Kadam, Y. R. Ma, S. S. Pujari and U. M. Patil, *J. Alloys Compd.*, 2021, **885**, 11.
17. D. Q. Yin, Z. Y. Jin, M. M. Liu, T. T. Gao, H. Y. Yuan and D. Xiao, *Electrochim. Acta*, 2018, **260**, 420-429.
18. Y. Zhang, T. T. Qu, F. F. Bi, P. P. Hao, M. H. Li, S. Y. Chen, X. K. Guo, M. J. Xie and X. F. Guo, *ACS Sustainable Chem. Eng.*, 2018, **6**, 16859-16866.
19. X. Y. Xu, H. Liu, D. D. Li, Q. C. Wang, X. J. Zhu, D. M. Liu and X. Chen, *J. Colloid Interface Sci.*, 2023, **650**, 498-505.